Supplemental Material

Supplementary information

1 Table of models

The list of 26 Coupled Model Intercomparison Project 5 (CMIP5) models that were used in this study. The columns denote, from left to right, the model index, the model name, its horizontal resolution (in degrees) and the number of atmospheric vertical levels. In all models, the high emissions representative concentration pathway 8.5 (RCP8.5) scenario is used for the projected runs, where the radiative forcing increases to about 8.5 W m^{-2} by the year of 2100. The historical runs include all the observed atmospheric forcing (including both anthropogenic and natural sources). For all models, the single run of ensemble member r1i1p1 is used. The data was obtained from the World Data Center for Climate (WDCC), available at http://cera-www.dkrz.de/WDCC/ui/.

Model index	Model name	Horizontal resolution (longitude$^\circ$ $\times$ latitude$^\circ$)	Vertical resolution (number of levels)
1	ACCESS1-0	1.9 $\times$ 1.2	38
2	ACCESS1-3	1.9 $\times$ 1.2	38
3	BCC-CSM1-1	2.8 $\times$ 2.8	26
4	BCC-CSM1-1-M	2.8 $\times$ 2.8	26
5	BNU-ESM	2.8 $\times$ 2.8	26
6	CanESM2	2.8 $\times$ 2.8	35
7	CCSM4	1.2 $\times$ 0.9	26
8	CMCC-CM	0.7$\times$ 0.7	31
9	CNRM-CM5	1.4 $\times$ 1.4	31
10	CSIRO-Mk3-6-0	1.9 $\times$ 1.9	18
11	FGOALS-g2	2.8 $\times$ 3.0	26
12	GFDL-CM3	2.5 $\times$ 2.0	48
13	GFDL-ESM2G	2.5 $\times$ 2.0	24
14	GFDL-ESM2M	2.5 $\times$ 2.0	24
15	HadGEM-CC	1.9 $\times$ 1.3	38
16	HadGEM-ES	1.9 $\times$ 1.3	60
17	INMCM4	2.0 $\times$ 1.5	21
18	IPSL-CM5A-MR	2.5 $\times$ 1.3	39
19	IPSL-CM5A-LR	3.8 $\times$ 1.9	39
20	MIROC5	1.4 $\times$ 1.4	40
21	MIROC-ESM	2.8 $\times$ 2.8	80
22	MIROC-ESM-CHEM	2.8 $\times$ 2.8	80
23	MPI-ESM-LR	1.9 $\times$ 1.9	47
24	MPI-ESM-MR	1.9 $\times$ 1.9	95
25	MRI-CGCM3	1.1 $\times$ 1.1	48
26	NorESM1-M	2.5 $\times$ 1.9	26

Table S1: List of 26 CMIP5 models included in this study, ordered alphabetically. Shown are the model index, name, horizontal resolution (in degrees) and the number of atmospheric vertical levels.

2 Vertical cross-section of extreme temperatures

Composite of the vertical cross-section for the strongest 25^{th} percentile warm and cold temperature anomalies in ERA-Interim is shown in Fig. S1. It is based on the tracking of 850 hPa temperature anomalies during DJF in the SH (see methods section in the manuscript for the full details). The vertical cross-sections show that a strong signal extends throughout the depth of the troposphere, especially at low levels, for both warm and cold temperature anomalies.

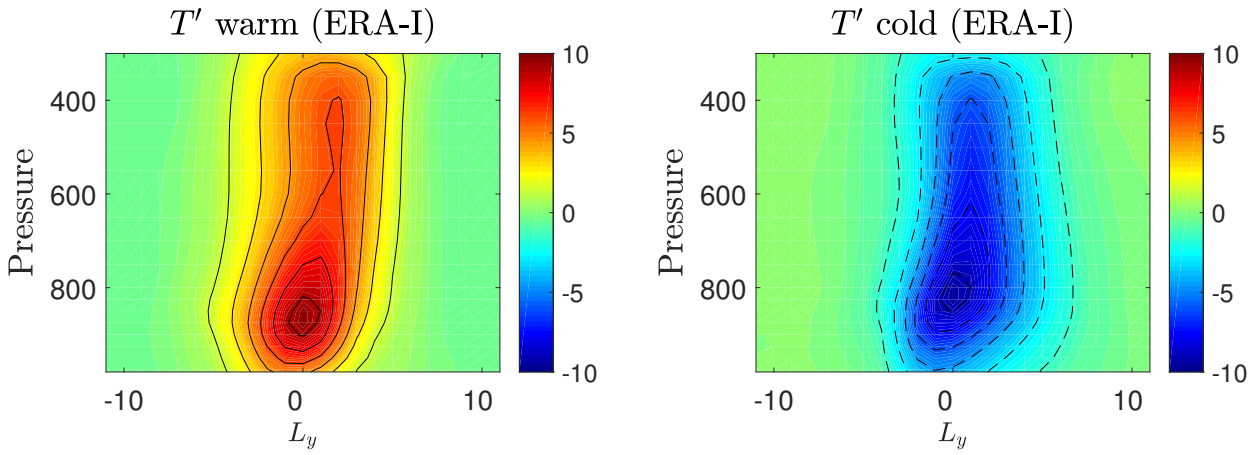

Figure S1: Composites of the vertical cross-section of temperature anomalies (in units K), produced by tracking the strongest 25^{th} percentile 850 hPa warm and cold temperature anomalies in the SH midlatitudes (30°S-70°S). The cross sections are taken at the longitude of maximum intensity (i.e., the middle of the composite box). The lowest contour equals 1.5 K, and the contour intervals equal 1.5 K. L_y denote the latitudinal distance (in degrees) from the center of the composite box.

3 Zonally averaged skewness

Fig. S2 shows the model spread of the zonally averaged skewness, from the 26 CMIP5 models participating in the study, where blue (red) lines denote the historical (projected) simulations. For each model, the maximum and minimum of the historical and projected skewness occur in a slightly different latitude, which is why when averaging latitudinally between fixed latitudes (e.g., dashed lines between 40°S to 55°S, and between 55°S to 70°S, as was done in Fig. 4 in the manuscript) the signal in the change is slightly muted. However, the general tendency can still be observed (see thick black solid and dashed lines that show the ensemble average for the historical and projected simulations, respectively): the overall poleward shift of the skewness structure implies that the positively skewed latitudinal band between 40°S to 55°S becomes less positively skewed, and the positively skewed latitudinal band between 55°S to 70°S becomes even more positively skewed.

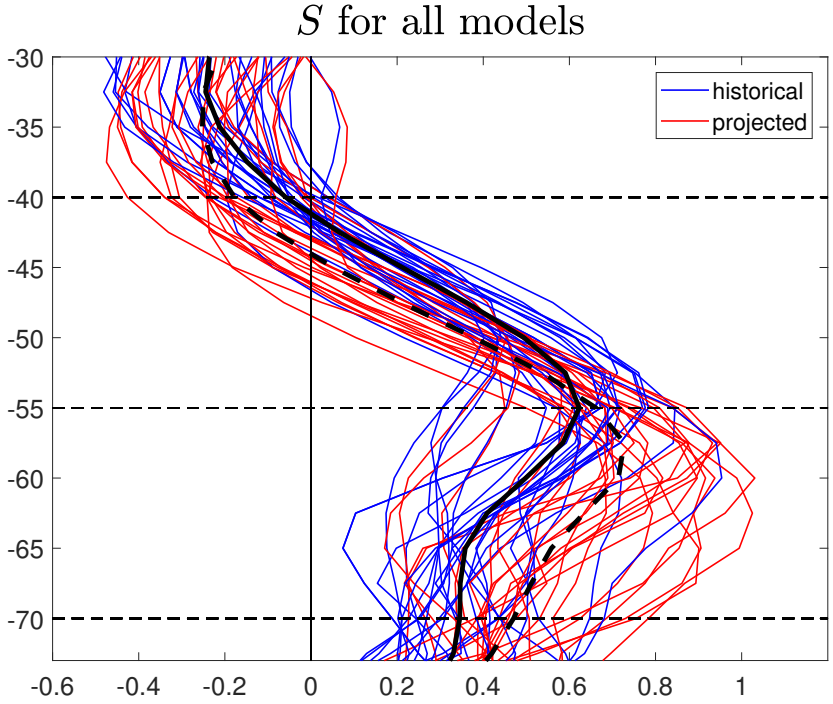

Figure S2: Model spread of zonally averaged skewness, from the 26 CMIP5 models participating in the study. The blue (red) lines show the historical (projected) zonally averaged skewness of each model, while the thick solid (dashed) black lines show the model mean zonally averaged skewness in the historical (projected) simulations. The thin black dashed lines at latitudes 40°S, 55°S, and 70°S denote the latitudes used for the band separation used in Fig. 4 in the manuscript.

4 Statistical significance assessment of skewness changes

A statistical significance assessment of the skewness change and model spread in the two latitudinal bands 40°S-55°S and 55°S-70°S is shown in Fig. S3. It is calculated in three different ways: from the zonally averaged skewness change in the corresponding latitudinal band of each model (Fig. S3a,b), from the zonally averaged change in the ratio of warm to cold temperature anomalies from the tracking (Fig. S3c,d), and from the skewness change of the temperature PDFs of each model (Fig. S3e,f). For each method, the 95% confidence interval of the mean was calculated and shown as the grey shaded region. In both latitudinal bands, the models agree robustly on the change of the sign, and the overall mean change is found significant. The 95% confidence interval of the ensemble mean change of the temperature PDFs (Fig. S3e,f) was used to estimate the error of the skewness change for each latitudinal band appearing in the legend of Figure 4 in the manuscript.

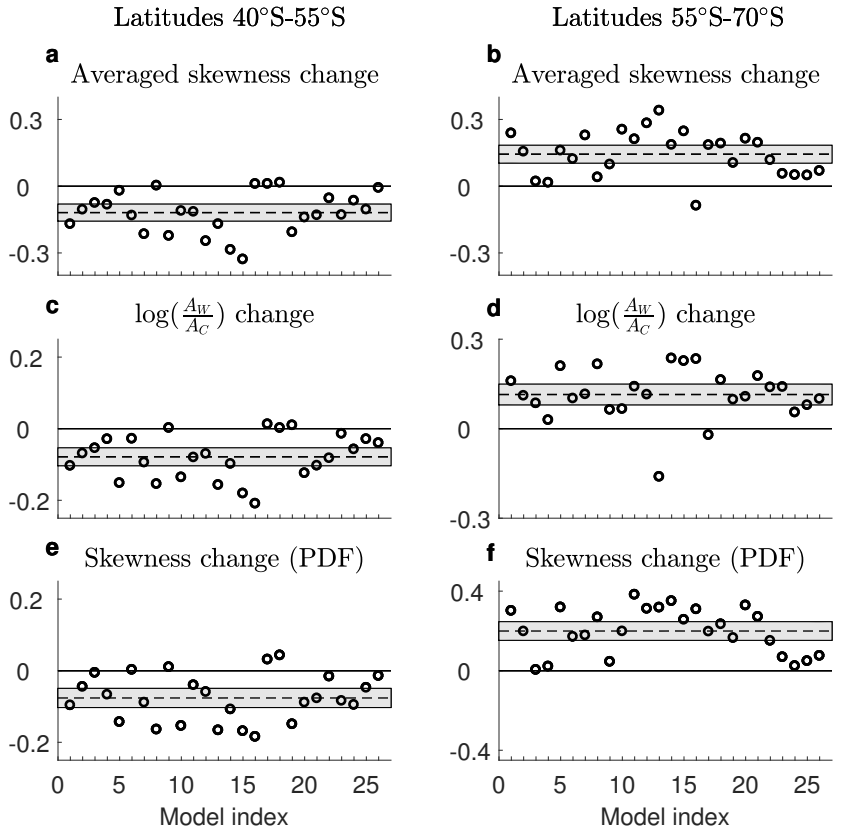

Figure S3: statistical significance assessment and model spread of the skewness change in the latitudinal bands 40°S-55°S (a,c,e) and 55°S-70°S (b,d,f), calculated for each model from (a,b) the zonally averaged Eulerian skewness change in the corresponding latitudinal band (c,d) the zonally averaged log of the ratio of mean intensity (absolute value) of warm anomalies to cold anomalies produced from the tracking, and (e,f) the skewness change of the temperature PDFs. Each dot corresponds to a model, and the model index on the abscissa is given in accordance with the list in Table S1. Dashed horizontal lines show the ensemble mean averages, and the shading denotes the 95% confidence interval of the mean (calculated as $\pm t_s \cdot SEM$, where $t_s \approx 0.26$ is taken from a t-test table with 26 degrees of freedom (number of models) and SEM is the standard error of the mean). In panels (c) and (d) the ratio is calculated on a log scale, such that the ratio is of equal magnitude if either $A_\mathrm{w} = 2A_\mathrm{c}$ or $A_\mathrm{c} = 2A_\mathrm{w}$ where A_w and A_c are the mean intensities of warm and cold anomalies, respectively.

5 Relative phase speed

Fig. S4 shows projected changes in the relative speed between the zonal mean jet and the zonal propagation of the temperature anomalies. In the CMIP5 ensemble mean, the zonal flow intensifies and shifts poleward, but so does the zonal eastward propagation of warm and cold anomalies (Fig. S4a and Fig. S4c, respectively). As a result, the zonal speed of temperature anomalies relative to the jet mostly decreases in the midlatitudes (Fig. S4b and Fig. S4d for the warm and cold anomalies, respectively). This is even more pronounced for the example model, MPI-ESM-LR (similarly but for panels e-h).

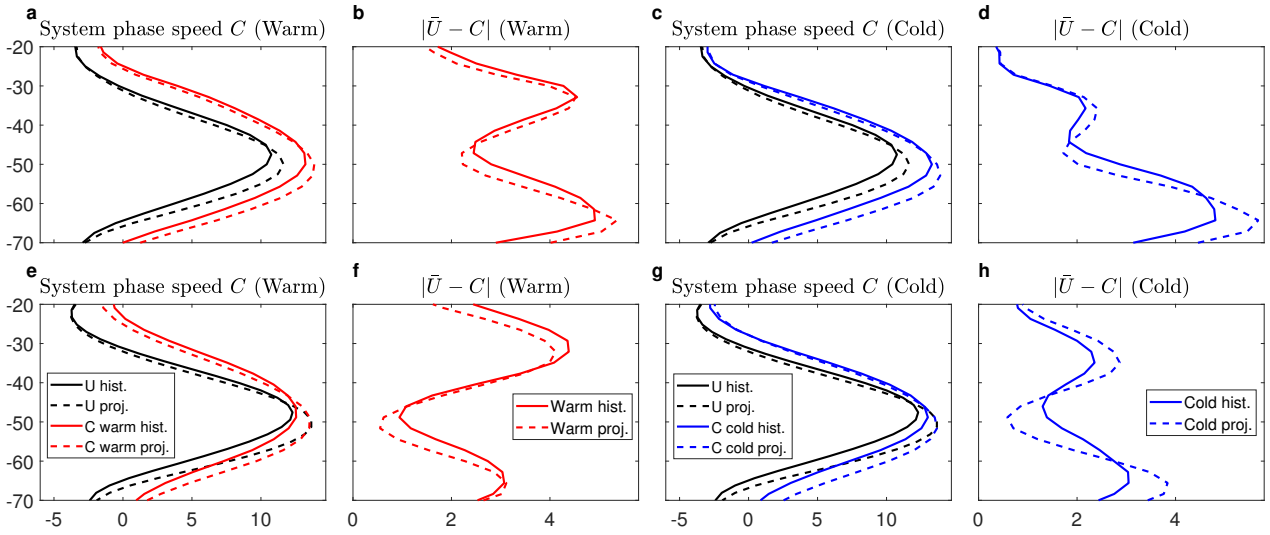

Figure S4: Projected changes in the relative speed between the zonal mean jet and the zonal propagation of temperature anomalies (ms^{-1}). Shown are the zonally averaged zonal mean flow and zonal speed of warm (a) and cold (c) anomalies from the tracking, and the difference between the zonal flow and the zonal speed of warm (b) and cold (d) anomalies, for the historical (solid) and projected (dashed) simulation of CMIP5. Panels (e)-(h) are the same but for the example model, MPI-ESM-LR.

6 Decrease in meridional displacements

Here we show the projected relative changes of the CMIP5 ensemble mean temperature variance (Fig. S5a), meridional background temperature gradient (Fig. S5b), and the variance of meridional displacements estimated from the linear approximation (Fig. S5c).

From the linear approximation one finds $\eta^2 = \overline{T'^2}/\overline{T}_y^2$, so the relative change in meridional displacements follows $\frac{\Delta(\eta^2)}{\eta^2} = \frac{\Delta(\overline{T'^2})}{\overline{T'^2}} - \frac{\Delta(\overline{T}_y^2)}{\overline{T}_y^2}$. Hence, changes in the meridional displacements depend both on temperature variance changes and on changes in the background gradient.

In the projected CMIP5 simulations both the temperature variance (Fig. S5a) and the meridional background temperature gradient (Fig. S5b) increase. However, the relative increase of the meridional temperature gradient in the midlatitudes is found to be larger than that of the temperature variance, consistent with $\overline{\eta^2}$ mainly decreasing there (Fig. S5c).

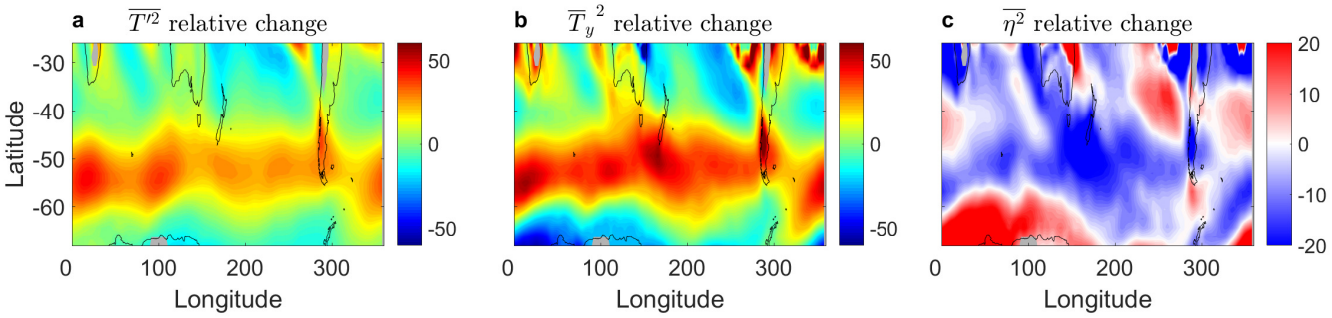

Figure S5: Ensemble mean relative projected changes of (a) temperature variance, (b) mean meridional temperature gradient, and (c) estimated meridional displacements, in percent.

7 Composites of nonlinear flux terms

Fig. S6 shows the composites of the nonlinear flux terms associated with warm and cold temperature anomalies. The composites show that the zonal flux term, $\frac{\partial(u'T')}{\partial x}$, is small compared to the meridional flux term, $\frac{\partial(v'T')}{\partial y}$, for both warm and cold anomalies. This motivated us to neglect $\frac{\partial(u'T')}{\partial x}$ in the derivation of the nonlinear approximation, given in Appendix A in the manuscript.

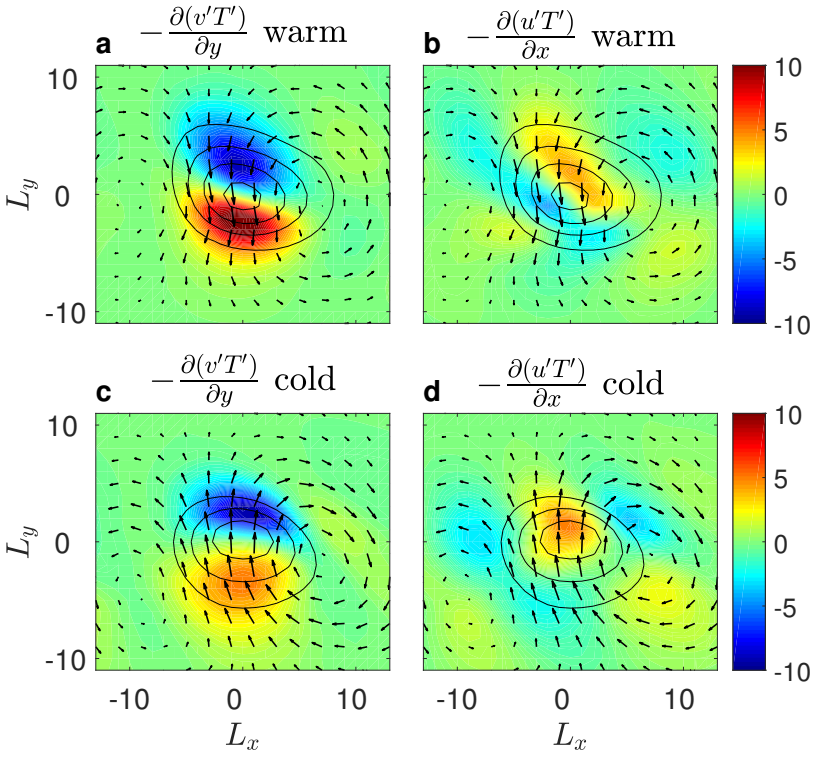

Figure S6: Composites of nonlinear flux terms (in units of $10^{-5}\mathrm{K}\cdot\mathrm{s}^{-1}$) at 850 hPa, following warm (a,b) and cold (c,d) anomalies in the SH. Shown are (a),(c) $-\frac{\partial(v'T')}{\partial y}$, and (b),(d) $-\frac{\partial(u'T')}{\partial x}$. The composites are produced by tracking the positive and negative 850 hPa temperature anomalies in ECHAM6 (MPI-ESM-LR), in the historical simulation. The black contours show the low level (850 hPa) temperature anomaly (where the lowest contour equals ± 2 K, and contour intervals equal ± 2 K), and the arrows show the corresponding anomalous velocity field in the composite. L_x and L_y denote the longitudinal and latitudinal distance (in degrees), respectively, from the center of the composite box.